Eur. Phys. J. B **55**, 229–235 (2007)
DOI: 10.1140/epjb/e2007-00050-6

THE EUROPEAN PHYSICAL JOURNAL B

Density-functional calculation of the quadrupole splitting in the ^{23}Na NMR spectrum of the ferric wheel Na@Fe$_6$(tea)$_6^+$ for various broken-symmetry states of the Heisenberg spin model

F.A. Bischoff[1,2], O. Hübner[3], W. Klopper[1,2,3,a], L. Schnelzer[4], B. Pilawa[1,4], M. Horvatić[5], and C. Berthier[5]

[1] Center for Functional Nanostructures (CFN), Universität Karlsruhe (TH), 76128 Karlsruhe, Germany
[2] Institut für Physikalische Chemie, Universität Karlsruhe (TH), 76128 Karlsruhe, Germany
[3] Institut für Nanotechnologie, Forschungszentrum Karlsruhe, Postfach 3640, 76021 Karlsruhe, Germany
[4] Physikalisches Institut, Universität Karlsruhe (TH), 76128 Karlsruhe, Germany
[5] Grenoble High Magnetic Field Laboratory, CNRS, Boîte Postale 166, 38042 Grenoble Cedex 9, France

Received 15 november 2006 / Received in final form 25 January 2006
Published online 16 February 2007 –

Abstract. The quadrupole splitting in the ^{23}Na nuclear magnetic resonance (NMR) spectrum of the hexanuclear ferric wheel Na@Fe$_6$(tea)$_6^+$ has been computed via an evaluation of the electric-field gradient (EFG) at the Na nucleus in the framework of density-functional theory (DFT). The simulated spectrum is compared with experimental data. A total of $2^6 = 64$ Kohn-Sham determinants (a number that reduces to eight symmetry-unique determinants due to the high S_6 symmetry of the ferric wheel) with six localised high-spin Fe(III) centres ($S = 5/2$) could be optimised in a self-consistent manner, and the corresponding DFT energies of all of these (broken-symmetry) determinants coincide almost perfectly according to the Ising Hamiltonian solutions, especially when the energy is computed from the B3LYP functional. The EFG at the Na atom does not depend much on the specific Kohn-Sham determinant but depends on the geometry of the ferric wheel and on the basis set used in the DFT calculations (particularly with regard to the atomic functions on the Na atom).

PACS. 31.15.Ew Density-functional theory – 33.25.+k Nuclear resonance and relaxation – 75.30.Et Exchange and superexchange interactions – 75.50.Xx Molecular magnets

1 Introduction

In recent years, a variety of molecules have been synthesized that exhibit molecular magnetism. Such molecules usually consist of between 6 and 18 transition-metal atoms coordinated by organic ligands [1]. The metal atoms have no direct chemical bond but interact via bridging oxygen atoms. Hexanuclear ferric wheels are prominent examples of such molecular magnets [2–4], and the present work is concerned with the hexairon(III) hexa(triethanolate)amine complex, or more precisely, with its derivatives Na@Fe$_6$(tea)$_6^+$ and Li@Fe$_6$(tea)$_6^+$ (cf. Fig. 1).

The magnetic properties and the ^{7}Li NMR spectra of these molecules have been studied in detail experimentally [5,6], and in the present work, we report the ^{23}Na NMR spectra and aim at a full computational ab initio description of the observed properties. In particular, we shall use density-functional theory to compute both the exchange-coupling constant J of the Heisenberg spin model and the electric-field gradient at the alkali atom (Li or Na), which we will use to simulate the quadrupole coupling splitting of the ^{23}Na NMR signal. For Li@Fe$_6$(tea)$_6^+$ the splitting is too small to be observed [6].

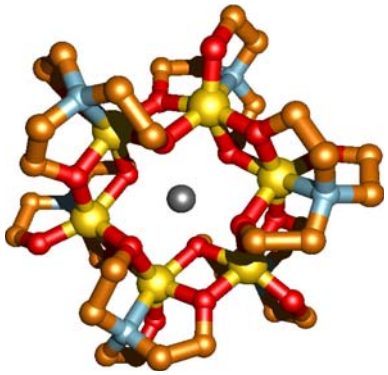

Fig. 1. Na@Fe$_6$(tea)$_6^+$, with all hydrogen atoms omitted for clarity. Colour legend: Na (grey), Fe (yellow), O (red), N (light blue), C (orange).

[a] e-mail: klopper@chem-bio.uni-karlsruhe.de

2 Theory

2.1 Exchange-coupling constant

The Heisenberg spin model (HSM) is appropriate for the description of the magnetism of a spin system such as the ferric wheel. The HSM Hamiltonian is

$$\hat{H} = -\sum_{i<j}^{N} J_{ij} \hat{\mathbf{S}}_i \cdot \hat{\mathbf{S}}_j, \tag{1}$$

where J_{ij} is the interaction strength (exchange-coupling constant) between the spin centres i and j, and $\hat{\mathbf{S}}_i$ and $\hat{\mathbf{S}}_j$ are the respective local spin operators. Second- and higher-order terms are assumed to be negligible [7,8]. If all nearest-neighbouring spin centres have the same interaction strength and all other couplings are negligible, the HSM can be simplified to

$$\hat{H} = -J \sum_{i=1}^{N} \hat{\mathbf{S}}_i \cdot \hat{\mathbf{S}}_{i+1}, \quad \hat{\mathbf{S}}_{N+1} = \hat{\mathbf{S}}_1. \tag{2}$$

Ideally, one would like to compute the low-lying electronic states of the molecular system by means of multireference wavefunction-based methods that include dynamic electron correlation effects. The electronic wavefunctions resulting from such calculations would be spin eigenstates, and one could compute a value for J by comparing the electronic energies with the eigenvalue spectrum of the Heisenberg Hamiltonian. An example of such a calculation on a dinuclear compound (as a model for the hexanuclear ferric wheel) has been reported very recently in this journal [9] (for earlier examples, see references therein).

Multireference wavefunction-based methods are not applicable, however, to large molecular systems such as the hexanuclear ferric wheel. Therefore, such systems are usually treated at the level of density-functional theory (DFT) by the broken-symmetry (BS) approach of Noodleman[7,10]. In this approach, one searches for the BS solution to the Kohn-Sham (KS) equations and compares the total energy of this solution with the energy of the high-spin (HS) state, which is typically well described by the corresponding KS determinant. There are formal problems with this approach related to whether or not BS solutions would exist if the exact exchange-correlation functional were used, whether or not one can evaluate expectation values of many-body operators such as $\langle \hat{S}^2 \rangle$ in DFT, and whether or not one should regard the HS-KS and BS-KS solutions as exact spin eigenstates. References [8] and [11] provide recent and comprehensive discussions of these issues.

In the present article, we follow the original BS approach of Noodleman. Using ladder operators, the HSM Hamiltonian can be written as

$$\hat{H} = -J \sum_{i=1}^{N} \Big[\frac{1}{2} \left(\hat{S}_{i+} \hat{S}_{(i+1)-} + \hat{S}_{i-} \hat{S}_{(i+1)+} \right) + \hat{S}_{iz} \hat{S}_{(i+1)z} \Big], \quad \hat{\mathbf{S}}_{N+1} = \hat{\mathbf{S}}_1. \tag{3}$$

Neglecting the ladder operators (i.e., assuming the overlap of different determinants to be zero), this leads to the Ising Hamiltonian

$$\hat{H}_{\mathrm{Ising}} = -J \sum_{i=1}^{N} \hat{S}_{iz} \hat{S}_{(i+1)z}, \quad \hat{S}_{(N+1)z} = \hat{S}_{1z}. \tag{4}$$

Within the usual spin-unrestricted KS calculations used in the BS approach, local high-spin centres are only realised by states with either all spins at one centre aligned downwards or all spins aligned upwards. For the case of N local high-spin centres, the operator $\hat{S}_{iz}$ yields $M_{S,\max} = S$ (all spins up) or $M_{S,\min} = -S$ (all spins down). The product $\hat{S}_{iz} \hat{S}_{(i+1)z}$ thus yields $-S^2$ for antiferromagnetically and $+S^2$ for ferromagnetically coupled neighbouring spin centres, and the expectation values of the Ising Hamiltonian for various Kohn-Sham determinants become

$$E = -J \sum_{i=1}^{N} M_{S_i} M_{S_{i+1}} = -J \left(P_{\mathrm{FM}} - P_{\mathrm{AF}} \right) S^2, \tag{5}$$

where P_{AF} and P_{FM} are the numbers of antiferromagnetically (AF) and ferromagnetically (FM) coupled neighbouring spin centres, respectively, and S is the total spin quantum number ($S = 5/2$) on each centre.

If the overlap between different spin centres is not negligible [12], the energy is given by

$$E = -J \left[\left(P_{\mathrm{FM}} - P_{\mathrm{AF}} \right) S^2 - \frac{1}{2} P_{\mathrm{AF}} \, \mathrm{Tr}(\mathbf{S}_{ab} \mathbf{S}_{ab}^T) \right], \tag{6}$$

with $\mathbf{S}_{ab}$ the overlap matrix containing all spatial overlap integrals between the magnetic orbitals on the AF-coupled centres a and b (in the present case, a 5×5 matrix).

Unfortunately, very different values for J are obtained with the BS approach for different popular DFT functionals. Former studies [9,13,14] have shown that the B3LYP functional works well in practice. Hartree-Fock theory fails completely (it does not even give the correct sign of J) and non-hybrid gradient-corrected methods tend to overestimate the value of J by a factor of 2 to 5. J can be determined experimentally by measurements of the static magnetic susceptibility. We have used the energy-conversion factor $1\ E_{\mathrm{h}} = 3.157\,746\,5(55) \times 10^5$ K.

2.2 Electric-field gradient

In the present article, we are primarily interested in the electric-field gradient (EFG) at the nucleus of the alkali atoms Na and Li in $\mathrm{Na@Fe_6(tea)_6^+}$ and $\mathrm{Li@Fe_6(tea)_6^+}$, respectively. The traceless EFG tensor at a point $\mathbf{K}$ is computed as a n-electron expectation value

$$\mathbf{V}_{\mathrm{EFG}} = \frac{1}{3} \sum_{i=1}^{n_{\mathrm{elec}}} \langle 0 | \frac{3 \mathbf{r}_{iK} \mathbf{r}_{iK}^T - \mathbf{r}_{iK}^T \mathbf{r}_{iK} \mathbf{I}}{r_{iK}^5} | 0 \rangle - \frac{1}{3} \sum_{A=1}^{n_{\mathrm{nucl}}} Z_A \frac{3 \mathbf{r}_{AK} \mathbf{r}_{AK}^T - \mathbf{r}_{AK}^T \mathbf{r}_{AK} \mathbf{I}}{r_{AK}^5}, \tag{7}$$

Table 1. Basis-set combinations.

Basis set	Alkali	Fe	N, O	C, H
SSSS	SVP	SVP	SVP	SV(P)
TSSS	TZVP	SVP	SVP	SV(P)
TTSS	TZVP	TZVP	SVP	SV(P)
QTSS	QZVP	TZVP	SVP	SV(P)
qTSS	dec-QZVP	TZVP	SVP	SV(P)
gTSS	ghost-dec-QZVP	TZVP	SVP	SV(P)
0TSS	None	TZVP	SVP	SV(P)
qTSSsf	dec-QZVPsf	TZVP	SVP	SV(P)
qTSSssf	dec-QZVPssf	TZVP	SVP	SV(P)
TTTS	TZVP	TZVP	TZVP	SV(P)
QTTS	QZVP	TZVP	TZVP	SV(P)

where $\mathbf{r}_{iK} = \mathbf{r}_i - \mathbf{K}$ is the vector from the point $\mathbf{K}$ to electron i, $\mathbf{r}_{AK} = \mathbf{r}_A - \mathbf{K}$ the vector from the point $\mathbf{K}$ to nucleus A, $|0\rangle$ the KS determinant, and $\mathbf{I}$ a 3×3 unit matrix.

The HS-KS and BS-KS states are represented by different KS determinants with different electron densities and thus yield different EFGs. As the EFG interacts with the nuclear quadrupole moment, it can be observed in the nuclear magnetic resonance (NMR) spectrum of the alkali atom. The EFG is sensitive to the geometric structure of the molecular system and can reveal effects such as Jahn-Teller distortions.

As the title molecule is an oblate symmetric top, the xx and the yy tensor elements of $\mathbf{V}_{\mathrm{EFG}}$ are identical while the zz element is twice as large in absolute value but with opposite sign. It is therefore sufficient to give only the zz element, which in the present work is reported in units of ma.u. $= 10^{-3}\ E_\mathrm{h}/(a_0^2 e) = 9.717\,361\,82(83) \times 10^{18}\ \mathrm{Vm}^{-2}$.

3 Methods

All calculations were carried out with the TURBOMOLE program package [15–17]. They were performed as spin-unrestricted KS calculations without imposing symmetry. The following exchange-correlation functionals were used: BP86 [18–21], B3LYP [18–20,22–24], TPSS [18,22,25,26], and TPSSh [18,22,25–27]. Basis sets were taken from the TURBOMOLE basis set library [28], and the abbreviations for various basis-set combinations are listed in Table 1. The prefix "dec" indicates a fully decontracted basis and the suffixes "sf" and "ssf" denote additional steep functions at the central alkali atom. When steep functions were added, they had the following exponents (obtained by multiplying the largest exponents of the original basis by 10 and 100): for Na, s: 37985220.08, 3798522.008, p: 69077.627017, 6907.7627017, d: 290, 29.0, f: 13.5, 1.35; for Li: s: 1485397.7085, 148539.77085, p: 326.051, 32.6051, d: 23.0, 2.30, f: 13.5, 1.35. Only the functions with the smaller of the two additional exponents were used for the sf basis sets, both extra functions were used for the ssf basis set. Other numerical parameters are: grid m4 for the numerical integration, thresholds of $10^{-8} E_\mathrm{h}$ for the self-consistent-field (SCF) convergence criterion and a Cartesian gradient of $10^{-4} E_\mathrm{h}/a_0$ for the geometry optimisations. All calculations were performed for the M@Fe$_6$(tea)$_6^+$ ion with M = Na, Li using the X-ray diffraction (XRD) structures of [2].

We applied the following procedure to obtain the BS solutions: first, the HS-KS calculation was performed with trial orbitals obtained from an extended Hückel calculation with 30 unpaired electrons. Then, for all the other BS-KS determinants, the valence orbitals of the HS-KS determinant were localised, an appropriate number of spins

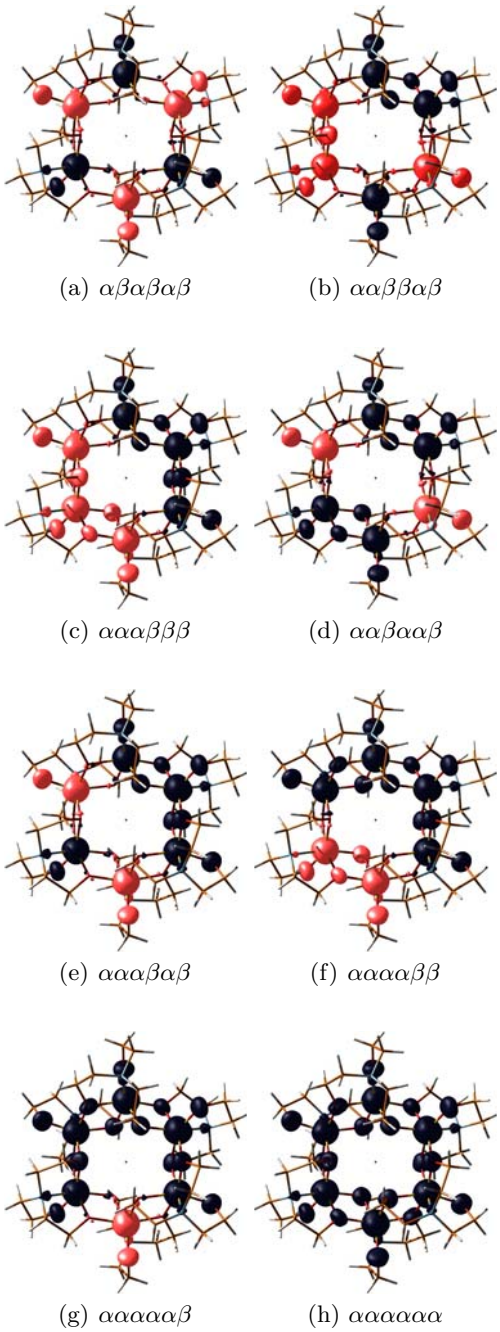

Fig. 2. Spin densities of the eight B3LYP/QTSS Kohn–Sham determinants of Table 3. Spin-up: blue, spin-down: red.

Table 2. Exchange-coupling constants and energy differences between the AF and the FM determinants of M@$Fe_6(tea)_6^+$ with M = Li, Na (experimental XRD structures).

Alkali	Basis	BP86		B3LYP		TPSS		TPSSh		Exp.
		$\Delta E/mE_h$	J/K	$\Delta E/mE_h$	J/K	$\Delta E/mE_h$	J/K	$\Delta E/mE_h$	J/K	J/K
Na	QTSS	−20.34	−85.6	−6.12	−25.8	−17.18	−72.3	−9.11	−38.4	
	QTTS	−21.76	−91.6	−6.93	−29.2	−18.45	−77.7	−10.03	−42.2	−23.0
Li	QTSS	−17.86	−75.2	−4.39	−18.5	−14.77	−62.2	−7.17	−30.2	
	TTTS	−19.22	−80.9	−5.15	−21.7	−15.09	−67.3	−8.04	−33.3	−18.1

in these localised orbitals were flipped. The resulting orbitals were used as an initial guess vector, which after SCF optimisation converged to the targeted BS-KS states. The spin densities of these states are depicted in Figure 2, showing that the correct BS-KS states were obtained by the localisation/spin-flipping procedure. The EFG was finally calculated using the script Moloch2.

4 Magnetic coupling

4.1 XRD structures

The exchange-coupling constant J, calculated with various functionals, is displayed in Table 2. ΔE denotes the energy difference between the AF and the FM determinant. We observe that very different results are obtained with the different functionals, but all carry the correct sign. The experimental value for Na@$Fe_6(tea)_6^+$ is −23 K [5]. Only the results using the B3LYP hybrid functional (−25.8 K in the QTSS basis) are close to this value, all the other functionals overestimate the magnitude of J. BP86 gives J values too large by about a factor of four (−85.6 K) and TPSS by about a factor of three (−72.3 K). Even the hybrid functional TPSSh overestimates the magnitude of J by almost a factor of two (−38.4 K). There is not much basis-set dependence. Only when the basis on the bridging O atoms is enlarged (as in the QTTS and TTTS basis sets), J increases by about 10% in magnitude for all functionals. This reflects the superexchange by the bridging O atoms.

The other determinants were also considered for Na@$Fe_6(tea)_6^+$ and were computed in the QTSS basis with the BP86 and the B3LYP functionals. By virtue of the symmetry of the molecule (almost S_6), there are only eight distinct determinants, including the AF and the FM states. Within the HSM, energies are easily evaluated and can be compared with those of the DFT calculations. The results are listed in Table 3. The relative energies ΔE with respect to the AF determinant are given in the first column of each functional entry. In the second column, the energy of the AF determinant was set to $+6JS^2$ and that of the FM determinant to $-6JS^2$, according to the HSM (Eq. (5)), and all the other values are given relative to these two. It appears that the B3LYP values fit much better to the HSM than those of BP86. Probably due to its more localised nature, the overlap $\mathrm{Tr}(\mathbf{S}_{ab}\mathbf{S}_{ab}^T)$ is much smaller in the case of B3LYP ($\approx 6.55 \times 10^{-3}$) than for BP86 ($\approx 3.7 \times 10^{-2}$), indicating that the mapping of the B3LYP functional onto the Heisenberg Hamiltonian is more justified than the mapping of BP86. This fact, and the superior values for J, are evidence that B3LYP is likely to give good exchange coupling constants. Inclusion of the overlap would decrease the magnitude of J, but the effect is negligible in comparision with other sources of error. In the special case of $Fe_6(tea)_6$, J decreases by about 0.025% with B3LYP and by 0.14% with the BP86 exchange-correlation functional. All of the values were obtained for the experimental XRD structure, which is not strictly S_6 symmetric, and the small deviations of the DFT energies from the Heisenberg model show that the model is valid for this molecule. As expected, all determinants, except that of FM, are heavily spin-contaminated as they are not pure spin states.

4.2 Optimised structures

The structures of the molecules were optimised for the FM and AF determinants, using different basis sets and functionals. As such optimisations are computationally demanding, not all possible combinations of functionals and basis sets were calculated. The geometry convergence was poor, indicating a shallow minimum or several local minima. Both optimised structures are larger than the XRD structures, independent of functional and basis set. In particular, the optimised distance of the nitrogen ligands from the Fe atom is consistently around 15 pm longer than in the XRD structure, indicating counterion and/or packaging effects. However, the Fe–O–Fe bonding angles are different for the three structures. The angles decreased from the XRD structure to the AF structure by roughly one degree and by another degree for the FM structure, depending on which oxygen atom defines the angle. The structures were nearly independent of the functional.

The results of the magnetic coupling calculations using the optimised structures are given in Table 4. For the optimised structures, we observe similar trends as for the XRD structures, but J is significantly smaller in absolute value than for the XRD structures. The reason for this decrease is the reduction in the bonding angles between the Fe atoms and the bridging oxygens and the simultaneous increase in the bond lengths. This leads to a weaker interaction between the Fe centres and thus to a stabilisation of the FM state. The AF state is also stabilised by relaxing the geometry but not as much as the FM state,

Table 3. Values of J for different determinants of $Na@Fe_6(tea)_6^+$ (QTSS basis, experimental XRD structure).

Determinant	BP86		B3LYP		Ising	M_S	$\langle\hat{S}^2\rangle$
	$\Delta E/mE_h$	$E/(JS^2)$	$\Delta E/mE_h$	$E/(JS^2)$	$E/(JS^2)$		
$\alpha\beta\alpha\beta\alpha\beta$	0	6	0	6	6	0	15
$\alpha\alpha\beta\beta\alpha\beta$	6.42	2.21	2.01	2.05	2	0	15
$\alpha\alpha\alpha\beta\beta\beta$	13.14	−1.76	4.04	−1.93	−2	0	15
$\alpha\alpha\beta\alpha\alpha\beta$	6.45	2.19	2.01	2.05	2	10	40
$\alpha\alpha\alpha\beta\alpha\beta$	6.58	2.21	2.02	2.03	2	10	40
$\alpha\alpha\alpha\alpha\beta\beta$	13.18	−1.78	4.04	−1.94	−2	10	40
$\alpha\alpha\alpha\alpha\alpha\beta$	13.36	−1.89	4.06	−1.97	−2	20	114
$\alpha\alpha\alpha\alpha\alpha\alpha$	20.34	−6	6.12	−6	−6	30	240

Table 4. Exchange-coupling constants and energy differences between the AF and the FM determinants of $M@Fe_6(tea)_6^+$ with M = Li, Na (DFT-optimised structures).

Alkali	Basis	BP86		B3LYP		TPSS		TPSSh	
		$\Delta E/mE_h$	J/K	$\Delta E/mE_h$	J/K	$\Delta E/mE_h$	J/K	$\Delta E/mE_h$	J/K
Na	SSSS	−15.32	−64.5	−4.40	−18.5	−13.30	−56.0	−7.03	−29.6
	QTSS	−17.16	−72.2	—	—	−15.13	−64.7	—	—
Li	SSSS	−14.09	−59.3	−3.39	−14.3	−11.62	−48.9	−5.60	−23.6
	QTSS	−15.85	−66.7	—	—	—	—	—	—

because of the decreasing bond angles. As the optimised structures of the different functionals are very similar, the reduction has a nearly constant factor of ≈ 0.75 [1,29].

5 Electric-field gradient

5.1 $Na@Fe_6(tea)_6^+$

The computed EFG at the Na atom of $Na@Fe_6(tea)_6^+$ is shown in Table 5. We observe small differences between the different functionals and configurations (AF or FM), but larger differences between the results obtained in different basis sets. When the basis set is increased, the magnitude of the EFG increases, for example from −24.5 ma.u. in the SSSS basis to −71.6 ma.u. in the QTSS basis (BP86 functional, FM state). However, a decontraction of the basis at the central Na atom reduces the EFG (−46.4 ma.u. in the qTSS basis). This latter value does not change when we add additional steep functions (qTSSsf basis), indicating that the results are close to the limit of a complete basis on Na. In the qTSSsf basis set, the functionals mutually differ by less than 8%. The enlargement of the basis at the O atoms that are the nearest neighbours to Na yields qualitatively the same effect as the decontraction of the Na basis, but to a smaller extent. If one removes the central sodium atom but leaves the basis set, the EFG vanishes nearly completely (FM, BP86/gTSS: $V_{zz} = +2.9$ ma.u.). All of the effects can be traced back to the polarisation of the Na atom. The SSSS basis is too small to cover such effects, they occur only with larger basis sets. Moreover, the Na basis must be decontracted to describe the electron density properly in the vicinity of the nucleus. The EFG is the curvature of the electrostatic potential at the Na nucleus and is sensitive to the electron density at that point in space. The effect of increasing the O basis set is similar to that of decontracting the Na basis, as they span the same space.

The computed EFG can be used to calculate the Sternheimer antishielding factor γ_∞ of the Na atom. Denoting the EFG with and without the central Na atom as V_{zz} and $V_{zz,0}$ respectively, $\gamma_\infty = 1 - V_{zz}/V_{zz,0}$ becomes +17(3) instead of the published value of −5.3(1) [30].

The optimised structure of $Na@Fe_6(tea)_6^+$ shows a significantly smaller EFG (bottom row in Tab. 5). During the optimisation, the distances of the nearest-neighbouring O atoms from the central Na atom increased by about 3%, while the Fe atom separation increased by only 1.5%. This means that the electrostatic potential becomes more spherically symmetric, causing the EFG to decrease in magnitude.

5.2 $Li@Fe_6(tea)_6^+$

In contrast to $Na@Fe_6(tea)_6^+$, $Li@Fe_6(tea)_6^+$ has only C_i symmetry. This implies that the xx and the yy elements of the EFG tensor are no longer identical. Furthermore, all values are very small (Tab. 6). As before, the different functionals yield similar results, and the same holds for the two spin states (FM and AF). The basis set dependence is somewhat different from $Na@Fe_6(tea)_6^+$. All basis sets give the same results except for the decontracted sets with additional steep functions (qTTSsf and QTTSssf). When the Li is removed (gTSS), only a small change in the EFG is observed. This can be understood in the context of a polarisability. Li is smaller and harder than Na, it is much less polarised by the surrounding molecule.

Table 5. $V_{\mathrm{EFG},zz}$-element of the traceless EFG tensor of $\mathrm{Na@Fe_6(tea)_6^+}$ in $10^{-3}\ E_\mathrm{h}/(a_0^2 e)$ (experimental XRD structure). In the last row, the notation "qTSS/SSSS" denotes that the the EFG was calculated in the qTSS basis set for a structure optimised in the SSSS basis.

	BP86		B3LYP		TPSS		TPSSh	
	FM	AF	FM	AF	FM	AF	FM	AF
SSSS	−24.5	−24.6	−33.5	−33.6	−27.4	−27.5	−29.9	−30.0
TSSS	−57.7	−58.4	−60.5	−60.9	−61.0	−61.7	−56.1	−56.6
TTSS	−65.3	−66.1	−66.0	−66.4	−67.4	−68.1	−61.0	−61.5
QTSS	−71.6	−72.3	−76.0	−76.4	−73.8	−74.5	−68.5	−69.0
qTSS	−46.4	−47.2	−48.6	−49.0	−50.2	−50.9	−48.0	−48.5
qTSSsf	−45.7	−46.4	−48.5	−48.9	−49.3	−49.9	—	—
TTTS	−64.1	−64.9	−65.1	−65.5	−66.5	−67.2	−60.1	−60.6
QTTS	−61.5	−62.2	—	—	−65.6	−66.2	−61.0	−61.0
gTSS	2.9	—	4.0	—	2.9	—	3.3	—
0TSS	1.3	—	2.4	—	1.2	—	1.7	—
qTSS/SSSS	−24.2	−36.8	−26.6	−34.8	−30.5	−42.5	−29.6	−39.0

Table 6. Elements of the diagonalised EFG tensor of $\mathrm{Li@Fe_6(tea)_6^+}$ in $10^{-3}\ E_\mathrm{h}/(a_0^2 e)$ (XRD structure).

	BP86, FM	BP86, AF	B3LYP, FM	B3LYP, AF
SSSS	−4.9/−0.5/5.4	−4.9/−0.5/5.4	−4.9/−0.6/5.5	−4.9/−0.7/5.5
QTSS	−5.4/−0.5/5.9	−5.4/−0.5/5.9	−5.1/−0.7/5.8	−5.1/−0.7/5.8
qTSS	−5.5/−0.5/6.0	−5.5/−0.5/5.9	−5.2/−0.7/5.9	−5.2/−0.7/5.9
qTSSsf	−3.9/−0.5/4.4	—	—	—
TTTS	−4.9/−0.7/5.6	−4.9/−0.7/5.5	−0.8/−4.9/5.7	−4.9/−0.8/5.7
QTTS	−5.1/−0.6/5.8	−5.1/−0.6/5.7	—	—
qTTS	−5.3/−0.6/6.0	−5.3/−0.6/5.9	—	—
qTTSsf	−3.8/−0.5/4.3	—	—	—
qTTSssf	−4.0/−0.5/4.5	—	—	—
gTSS	−2.6/−1.0/3.7	—	—	—
qTSS/SSSS	−1.6/0.6/1.1	−1.9/0.7/1.2	−0.9/−0.3/1.2	−0.7/0.2/0.5
	TPSS, FM	TPSS, AF	TPSSh, FM	TPSSh, AF
SSSS	−5.2/−0.3/5.5	−5.2/−0.3/5.5	−5.1/−0.4/5.5	−5.1/−0.4/5.5
QTSS	−6.1/−0.0/6.1	−6.1/0.0/6.1	−5.9/−0.2/6.0	−5.9/−0.1/6.1
qTSS	−5.9/−0.1/6.0	−5.9/−0.1/6.0	−5.7/−0.2/6.0	−5.8/−0.2/6.0
TTTS	−5.0/−0.5/5.5	−5.0/−0.5/5.5	−4.9/−0.6/5.5	−4.9/−0.6/5.5
qTSS/SSSS	−1.6/0.5/1.2	−2.8/1.3/1.5	−0.9/0.4/0.5	−2.2/0.0/1.3

When relaxing the molecule the EFG changes significantly, similar to $\mathrm{Na@Fe_6(tea)_6^+}$. However, the resulting numbers are too small and too uncertain for any conclusions to be drawn.

5.3 NMR spectra

The ^{23}Na NMR ($I = 3/2$, $\gamma_0/2\pi = 11.2615$ MHz/T, $Q = +109(3) \times 10^{-31}$ m^2 [31]) measurements were performed at the GHMFL with a pulsed NMR spectrometer at 0.44 K. The $\mathrm{Na@Fe_6(tea)_6Cl}$ sample was mounted together with a metallic ^{27}Al ($\gamma_\mathrm{Al}/2\pi = 11.094$ MHz/T, $K = 0.161\%$) frequency reference in a dilution refrigerator. The orientation of the molecular symmetry axis with respect to the static magnetic field could not be determined before the experiment. The ^{23}Na spectra were measured with a 2 pulse $\pi/2 - \tau - \pi$ echo sequence ($\pi/2$ pulse length was 10 μs). Figure 3 shows the spectrum recorded at $B_0 = 10.5$ T. Accurate measurements of the line position were carried out at $B_0 = 10.4938$ T ($\nu_{0,\mathrm{Al}} = 116.6057$ MHz). The frequency of the central line ($+1/2 \leftrightarrow -1/2$ transition) was $\nu_c = 118.1870$ MHz, and for the high (H) and low (L) frequency quadrupole satellites ν_H and ν_L ($+1/2 \leftrightarrow +3/2$, and $-1/2 \leftrightarrow -3/2$ transitions) 118.3060 MHz and 118.0706 MHz, respectively.

For a quantitative analysis of the NMR spectra, the frequency of the three NMR lines can be calculated in the case of the axial symmetry of the hexa-nuclear iron ring for a given orientation ϑ of the external magnetic field, according to [32,33]

$$\nu_c = \nu_z + \Delta\nu^{(2)}_{Q_{1/2}} \tag{8}$$

for the central transition, and

$$\nu_{\mathrm{H,L}} = \nu_z + \Delta\nu^{(2)}_{Q_{3/2}} \pm |\Delta\nu_Q| \tag{9}$$

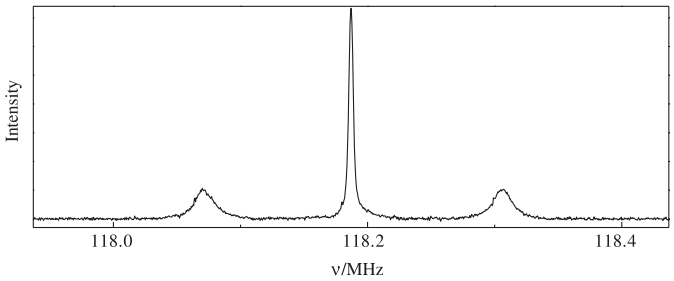

Fig. 3. Na-NMR single-crystal spectrum of $Na@Fe_6(tea)_6^+$ measured at 440 mK and $B_0 = 10.5$ T.

for the high and low frequency quadrupole satellites. Here,

$$\nu_z = \nu_{0,z}\,(1+\delta)\,, \tag{10}$$

with $\nu_{0,z} = (\gamma_0/2\pi)B_0$ and the chemical shift δ ($\sim$94 ppm),

$$\Delta\nu_Q = \tfrac{1}{2}\nu_Q\left[3\cos^2\vartheta - 1\right] \tag{11}$$

with $\nu_Q = e^2qQ/2h$ and the EFG $eq = V_{zz}$,

$$\Delta\nu^{(2)}_{Q_{1/2}} = -\frac{3\nu_Q^2}{16\nu_z}\left(1-\cos^2\vartheta\right)\left(9\cos^2\vartheta - 1\right), \tag{12}$$

and

$$\Delta\nu^{(2)}_{Q_{3/2}} = +\frac{3}{2}\frac{\nu_Q^2}{\nu_z}\left(1-\cos^2\vartheta\right)\cos^2\vartheta. \tag{13}$$

With the experimental results, the first-order quadrupolare splitting becomes $\Delta\nu_Q = 117.7$ kHz and the second-order correction $\delta_{\rm H} = \nu_{\rm H} - \nu_c - \Delta\nu_Q = \Delta\nu^{(2)}_{Q_{3/2}} - \Delta\nu^{(2)}_{Q_{1/2}} = 1.3(2)$ kHz. There are two possible solutions for these numbers. The orientation of the molecular symmetry axis is either $\vartheta_1 = 45.0(8)^\circ$ and $\nu_{Q,1} = 470(40)$ kHz or $\vartheta_2 = 62.8(8)^\circ$ and $\nu_{Q,2} = 630(60)$ kHz. With $\nu_Q = e^2qQ/2h$ the corresponding electric-field gradients are $V_{zz,1} = 3.57(32)\cdot 10^{20}$ V/m^2 and $V_{zz,2} = 4.78(44)\times 10^{20}$ V/m^2 (the sign of V_{zz} cannot be determined in the experiment). The experimental results have to be compared with the computed EFG (AF determinant, qTSS basis, XRD structure, average of the four functionals) $|V_{zz}| = 48.9(1.5)$ ma.u. $= 4.75(15)\times 10^{20}\,\mathrm{V/m^2}$. This value agrees especially well with the second solution of the experimental data and indicates that the orientation of the molecular axis during the experiment was $\vartheta_2 = 62.8(8)^\circ$.

This research has been supported by the Deutsche Forschungsgemeinschaft (DFG) through the Center for Functional Nanostructures (CFN, Project Nos. C3.3 and C3.7). It has been further supported by a grant from the Ministry of Science, Research and the Arts of Baden-Württemberg (Az: 7713.14-300). The authors thank Stephan Bischoff for preparing Figure 2.

References

1. B. Pilawa, Ann. Phys. **8**, 191 (1999)
2. R.W. Saalfrank, I. Bernt, E. Uller, F. Hampel, Angew. Chem. Int. Ed. **36**, 2482 (1997)
3. A. Cornia et al., Angew. Chem. Int. Ed. **38**, 2264 (1999)
4. B. Normand, X. Wang, X. Zotos, D. Loss, Phys. Rev. B **63**, 184409 (2001)
5. B. Pilawa et al., Phys. Rev. B **71**, 184419 (2005)
6. A. Lascialfari et al., J. Appl. Phys. **95**, 6879 (2004)
7. L. Noodleman, D.A. Case, Adv. Inorg. Chem **38**, 423 (1992)
8. I. de P.R. Moreira, F. Illas, Phys. Chem. Chem. Phys. **8**, 1645 (2006)
9. H. Nieber, K. Doll, G. Zwicknagel, Eur. Phys. J. B **51**, 215 (2006)
10. L. Noodleman, J. Chem. Phys. **74**, 5737 (1981)
11. I. Rudra, Q. Wu, T. Van Voorhis, J. Chem. Phys. **124**, 024103 (2006)
12. R. Caballol et al., J. Phys. Chem. A **101**, 7860 (1997)
13. A.V. Postnikov, S.G. Chiuzbăian, M. Neumann, S. Blügel, J. Phys. Chem. Sol. **65**, 813 (2004)
14. H. Nieber, K. Doll, G. Zwicknagel, Eur. Phys. J. B **44**, 209 (2005)
15. R. Ahlrichs et al., Chem. Phys. Lett. **162**, 165 (1989)
16. K. Eichkorn et al., Chem. Phys. Lett. **242**, 652 (1995)
17. K. Eichkorn, F. Weigend, O. Treutler, R. Ahlrichs, Theor. Chem. Acc. **97**, 119 (1997)
18. P.A.M. Dirac, Proc. Royal Soc. (London) **123**, 714 (1929)
19. S.J. Vosko, L. Wilk, N. Nusair, Can. J. Phys. **58**, 1200 (1980)
20. A.D. Becke, Phys. Rev. A **38**, 2098 (1988)
21. J.P. Perdew, Phys. Rev. B **33**, 8822 (1986)
22. J.C. Slater, Phys. Rev. **81**, 385 (1951)
23. C. Lee, W. Yang, R.G. Parr, Phys. Rev. **37**, 785 (1988)
24. A.D. Becke, J. Chem. Phys. **98**, 5648 (1993)
25. J.P. Perdew, Y. Wang, Phys. Rev. B **45**, 13244 (1992)
26. J. Tao, J.P. Perdew, V.N. Staroverov, G.E. Scuseria, Phys. Rev. Lett. **91**, 146401 (2003)
27. V.N. Staroverov, G.E. Scuseria, J. Tao, J.P. Perdew, J. Chem. Phys. **119**, 12129 (2003)
28. F. Weigend, R. Ahlrichs, Phys. Chem. Chem. Phys. **7**, 3297 (2005)
29. Y.-Q. Zhang, C.-L. Luo, Z. Yu, Int. J. Quant. Chem. **102**, 165 (2004)
30. H. Chihara, N. Nakamura, *Nuclear Quadrupole Resonance Spectroscopy Data*, *Landolt-Börnstein - Group III Condensed Matter* (1997), Vol. 39
31. D. Sundholm, J. Olsen, Phys. Rev. Lett. **68**, 927 (1992)
32. T.P. Das, E.L. Hahn, *Solid State Physics*, edited by F. Seitz, D. Turnbull (Academic Press, New York, 1958), Suppl. 1
33. G.C. Carter, L.H. Bennett, D.J. Kahan, *Progress in Materials Science*, edited by B. Chalmers, J.W. Christian, T.B. Massalski (Pergamon Press, Oxford, 1977), Vol. 20